

**Molecular rectifiers based on five-coordinate iron(III)-
containing surfactants**

Journal:	<i>Dalton Transactions</i>
Manuscript ID	DT-PER-07-2018-002891.R1
Article Type:	Perspective
Date Submitted by the Author:	27-Aug-2018
Complete List of Authors:	Verani, Claudio; Wayne State University, Chemistry

Molecular rectifiers based on five-coordinate iron(III)-containing surfactants

Received 00th January 20xx,
Accepted 00th January 20xx

Cláudio N. Verani^{*,a}

DOI: 10.1039/x0xx00000x

www.rsc.org/

In this article we review the state-of-the-art of metallorganic-based molecular rectification with an emphasis on our research in five-coordinate Fe^{III}-containing surfactants. We place rectification in the broader context of molecular electronics, and include the description of methodology used in electrode|LB film|electrode assemblies, concluding with an outlook on future directions for metallosurfactants.

Dedicated to Prof. Robert Metzger on the occasion of his 78th birthday

Molecular electronics and metal complexes

The search for molecule-based electronics began in the 1950s¹ with a US Airforce/Westinghouse joint program, von Hippel's molecular engineering approach, Fernbach and Proctor's use of spins for memory devices, and Feynman's talk² on the "problem of controlling things on a small scale". In 1965 Moore³ discussed the expected limitations imposed by heat dissipation resulting from component miniaturization, and by fabrication methods, where "the complexity for minimum component costs increases at a rate of roughly a factor of two per year..." Over the last five decades several approaches have been considered and adopted in order to address this issue. The use of single molecules, or small groups thereof, as replacements for solid state electronic components led to the development of an entirely new research field known as molecular electronics.⁴⁻⁷ Along with this research came the development of synthetic, analytical, and physical methods that delivered unique molecular systems with customized and controlled properties.⁸⁻¹⁰ Nonetheless, unfulfilled and unrealistic expectations curbed the enthusiasm on molecular electronics and by the mid-2000s the field had dwindled into academic curiosity. Renewed interest became obvious by the beginning of the 2010s.¹¹ The major emphasis was on purely organic systems, due to the facility of electron transport through delocalized 2p orbitals in planar and aromatic scaffolds. However, the appeal of metal-containing coordination complexes has been noticeable.^{12, 13} The most frequently used motifs include modified phthalocyanins, porphyrins, polypyridines, or ferrocenes (Figure 1). These ligands retain similar properties such as aromaticity and electron delocalization, although other systems have appeared after 2010 adding diversity to the field. As early as 1994 Pietro¹⁴ reported on

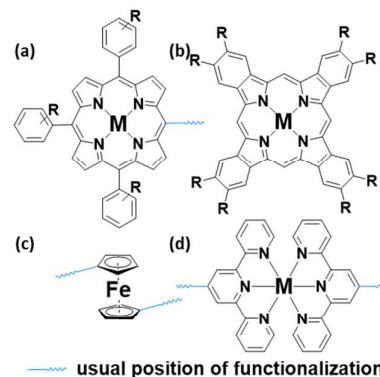


Figure 1. Usual coordination complexes in molecular electronics: (a) porphyrins, (b) phthalocyanins, (c) ferrocenes, and (d) terpyridines.

"non-Schottky-type" multilayer diodes based on Ni²⁺ and Cu²⁺ phthalocyanins, and in 1997 "short-circuit free LB sandwiches" based on phthalocyanins and perylene derivatives were reported.¹⁵ These bicomponent species were studied in great detail by the groups of Ashwell¹⁶ and Marks.¹⁷ Through the diligent work of Lindsey & Bocian^{18, 19} over the last decade, lanthanide-containing metalloporphyrins were shown to be bistable redox-based memory elements with high charge density and robustness to withstand circuitry processing. In 2002 a Cornell-based consortium published work²⁰ on electronic blockades and effects in single-molecule transistors based on Co^{II}/terpyridine species described as [Co^{II}(S-terpy)₂]. Electron transport was observed as a sigmoidal (S-shaped) response between current (*I*) and potential (*V*) in *I/V* curves and attributed to the Co^{II}/Co^{III} conversion. The coupling between the metal and the gold electrodes was controlled by the length of the alkyl chains between the terpyridine moiety and the self-assembling thiol group. Whereas a complex with pentacyl spacers showed an increased resistance that prevented current flow associated with small bias voltages known as Coulomb blockade, another complex

^a Department of Chemistry, Wayne State University, 5101 Cass Ave. Detroit Michigan, 48310, USA.
E-mail: claudio.verani@wayne.edu

with a thiol directly installed to the terpy unit showed a sudden temperature-dependent increase in current levels known as the Kondo effect. Similar thiol-tethered Ru^{II}-based terpyridine systems were used by the Lee group²¹ in 2008 for a voltage-driven molecular switch and used in solid-state molecular junctions. When a negative sample-bias was applied, the threshold voltage to the high conductance state in the molecular junctions of the Ru^{II} complex was consistent with the electronic energy gap between the Fermi level of the gold substrate and the lowest ligand-centered redox state of the metal complex molecule.²² Ferrocene-based systems appeared with the pioneering work by Gorman *et al.*^{23, 24} on the relative stochastic conductance at the nanoscale and attenuation of negative differential resistance of ferrocene anchored on gold using scanning tunneling microscopy.

More recent reports still rely on the ligands described in **Figure 1**, while expanding on ligand design and evidencing the prominence of coordination complexes^{25, 26} in molecular electronics:

(i) Electron transport was studied by Mayer *et al.*²⁷ focusing on intramolecular interactions in Au|cysteamine-ferrocene-cysteamine|Au assemblies indicating that covalency yields more efficient transport, while Higgins *et al.*²⁸ studied metal|conjugated molecule|metal assemblies, and proposed that, due to loss of coherence, longer molecules favor hopping²⁹ over tunneling. Rigaut summarized progress in this field.³⁰

(ii) The development of logic devices included the work of van der Boom *et al.*³¹ on molecular approaches for sequential logic, Metzger *et al.*³² on three-terminal unimolecular amplifiers for power gain, and Szacilowski *et al.*³³ on photoelectrochemical logic devices capable of performing basic ternary logic operations.

(iii) The building of molecular memory elements expanded from Lindsey & Bocian's porphyrin approach³⁴ to dialkylthiolate-tethered metal terpyridine self-assembled monolayers, used as nonvolatile memory and characterized by charge retention time that enables write/multiple read/erase/multiple read pulse cycles by the Lee group,²² as well as the use of photoresponsive films composed of sequential heterolayers based on Ru complexes.³⁵

(iv) Memristors,³⁶ the hypothetical two-terminal electrical component proposed in 1971 by theorist Leon Chua, and able to associate electric charge readings with magnetic flux were also investigated; Higushi *et al.*³⁷ described a unique memristive device based on a polymer-bound Co^{III} complex with an extended azaromatic ligand, where bistable on/off states support random flip-flop turning for several hours.

(v) On/off switches were studied by Goswami *et al.*³⁸ using azo-anion diradical complexes of Rh^{III} to show memory switching properties suitable for RAM/ROM applications, while the groups of Kume and Nishihara,³⁹ as well as van der Zant and Coronado⁴⁰ probed a reversible Cu^{II/I} species capable of light-induced ring rotation based on the changes of the ligand field around the 3d⁹ and 3d¹⁰ states. The Szacilowski group⁴¹ used Ru^{II}-containing polypyridine complexes chemisorbed onto TiO₂ surfaces to demonstrate the feasibility of photocurrent switching necessary for the development of optoelectronic logic devices.

(vi) The field of spintronics also received keen interest, and was summarized in a 2015 review by an international consortium led by Lloret and Julvea⁴² that included molecular magnetic couplers, capacitors, rectifiers, and wires,

While this short list is incomplete, it includes several examples of molecules acting as conductors, memory elements, transistors, and other components fundamental for computing processes. In these systems the metal is invariably confined to tetrahedral or octahedral ligand fields. The concept of a diode-like molecule capable of current rectification is detailed in the next section as relevant for background and contextualization of our own research.

Molecular rectification

Rectification is the diode-like property of modulating an asymmetric flow of electric current, or, transferring electrons in a unidirectional way. In macroscopic electrical circuitry, rectifiers such as vacuum tubes and solid-state diodes control the mobility of current, thus enabling electrons to flow in one direction from a given point A to a point B, while preventing reversibility from point B to point A. This directionality is fundamental to the conversion of alternating current (AC) into direct current (DC). Seeking alternatives to Moore's law, Metzger & Panetta⁴³ considered in 1973 the experimental possibility of molecule-based current rectification. A contemporaneous and more complete theoretical treatment to the problem came from Aviram and Ratner⁴⁴ in the form of an idealized single molecule placed in a junction⁴⁵ comprised of electrode|molecule|electrode. Central to this paradigm is the existence of asymmetric molecules that incorporate σ -bridged (-b-) electron-donor (D) and electron-acceptor (A) moieties, forming a [D-b-A] molecule with an excited state [D⁺-b-A⁻] of higher but accessible energy.⁴⁶⁻⁴⁹ Rectification is measured by the changes in current (*I*) with changing potential (*V*) of such molecules deposited between two electrodes and achieved as asymmetric and non-sigmoidal *I/V* curves. This response differs dramatically from sigmoidal *I/V* curves associated with conductivity, where current flows freely across the molecule. It also differs from flat *I/V* curves that indicate absence of current due to insulating molecules. **Figure 2** summarizes these 3 distinct kinds of behavior. In this electrode|molecule|electrode construct the donor and acceptor moieties of a hypothetical molecule (**Figure 3a**) must be separated by a σ -bridge that decreases electronic coupling, preventing internal charge transfer from donor to acceptor.⁵⁰

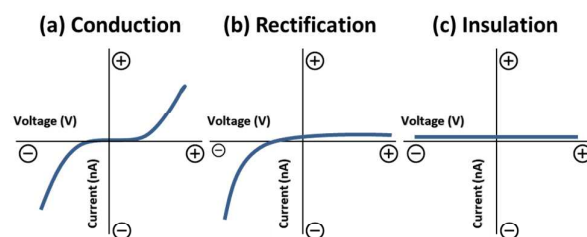


Figure 2. Distinct profiles of current change over applied potentials in *I/V* curves: (a) conducting, (b) rectifying, and (c) insulating behavior.

However, rectification was only achieved experimentally in the 1990s by Ashwell *et al.*^{51, 52} using a π -bridged hexadecylquinolinium-tricyanoquinodimethanide ($C_{16}H_{33}Q-\pi-3CNQ$) system (**Figure 3b**). The rectification behavior was later verified and optimized by Metzger,⁵³ as described in a series of elegant reviews.^{10, 43, 54-58}

Although single molecule conductance experiments have received attention in recent times,⁵⁹⁻⁶⁴ the use of SAMs and thin films has been an equally reliable. Here we focus on the latter.

Original work of Ashwell, Sambles, and Metzger observed rectification in devices containing monolayers or multilayers of the surfactant molecule $C_{16}H_{33}Q-\pi-3CNQ$. These early results showed the viability of Langmuir-Blodgett (LB) film deposition to yield compact and defect-free physisorbed films onto a solid substrate, thus spearheading the development of redox-active surfactants. It also raised questions about the mechanisms by which such molecular rectification takes place. At least our main mechanisms can contribute to current rectification, namely Schottky, environment polarization, asymmetric, and unimolecular mechanisms. Schottky rectification is based on interfacial dipoles between dissimilar electrodes or on covalent bonding between a self-assembled molecule and the electrode.⁶⁵⁻⁶⁷ As recently as in 2015, the Venkataraman group⁶⁸ has reported on a new environment-based mechanism on asymmetric polarization of single-molecule junctions; polar ionic solutions induce asymmetric changes in the electrostatic surroundings of a molecule, thus leading to alterations in the conductance.

We focus on asymmetric and unimolecular mechanisms; these mechanisms rely on the use of the highest occupied (HOMO) and lowest unoccupied (LUMO) frontier molecular orbitals for electron transfer. The former relies on an asymmetric placement of the frontier orbitals in the electrode|molecule|electrode assembly in which the HOMO is closer to one electrode and the LUMO (**Figure 3c**) is closer to the other, allowing for directional current flow.^{64, 69} Williams and Whitesides have proposed that the HOMO alone can carry the process⁷⁰. On the other hand, the unimolecular mechanism has two variants; it was originally accepted that electrons would travel $M_1 \leftarrow M_2$ when the molecule is in the ground state [D^0-b-A^0] and the electrode M_2 transfers an electron to A_{LUMO} , while the electrode M_1 receives one electron from D_{HOMO} . The excited electron in A_{LUMO} then relaxes to D_{HOMO} in an intramolecular electron transfer process (**Figure 3d**). Alternatively (and more commonly) an applied bias leads to the formation of the zwitterionic [D^+-b-A^-] that transfers an electron from A_{LUMO} to M_2 , followed by M_1 to D_{HOM} . In this case the transport involves $M_1 \rightarrow M_2$. While experimental distinction between asymmetric and unimolecular contributions can be ambiguous, there is consensus that electroactive molecules with local low-symmetry⁷¹⁻⁷³ constitute good candidates for the enterprise, and well-documented cases of molecular rectification rely heavily on the formation of high-quality LB monolayers.⁷⁴⁻⁷⁸ The inclusion of transition metal complexes in current rectification has received increasing attention. Besides the work of Pietro described above, Ren *et al.*⁷⁹ published in 2007 the use of bis-alkynyl Ru_2 species containing donor and acceptor groups on opposite ends of the molecule yielded an energetic alignment of

the frontier orbitals accepted as favoring directional electron flow. In 2008 the Yu group⁸⁰ studied the complex [ArS -bipy $Ru^{II}(F^3acac)_2$], in which a ruthenium(II) ion is coordinated to a thiophene-functionalized bipyridine and two fluorinated acetylacetonates. They observed that electron transport in the complex is more efficient than in the unmetallated ligand, due to the ligand planarity acquired upon metallation that facilitates conjugation. The rectification effect was tentatively explained by the presence of a permanent dipole moment perpendicular to the thiophene-functionalized bipyridine and along both fluorinated acac ligands, being mediated through the HOMO, HOMO-3, and HOMO-4 orbitals associated with the t_{2g} set (d_{xy}, d_{yz}, d_{zx}) of the Ru^{II} ion. In 2017 Chen *et al.*⁸¹ reported on a new Au|PDIBA-n|Au diode, where DIBA is an azulene derivative coordinated to Co^{II} and forming an extended coordination framework thin film prepared *via* layer-by-layer dip-coating. The rectifier displayed an average rectification ratio (*RR*) of 6 over 300 cycles. Other relevant works were published recently relying on the usual building blocks. Porphyrin-based systems were investigated by the Yale collaborative,⁸² which probed interfacial linkers between high-potential porphyrins and semiconductor surfaces via a series of different linkers and anchoring groups. Ogawa *et al.*⁸³ explored a different approach in which donating Zn^{II} or Rh^{II} porphyrins are bound perpendicularly to accepting naphthalene-1,4,5,8-bis(dicarboximide). While these studies were rather rigorous in their synthetic and quantum components, no actual measurement of the rectification ratios was offered.

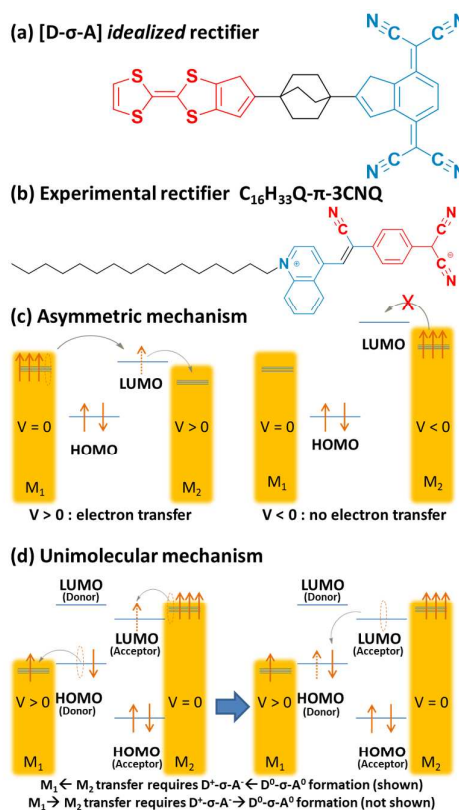


Figure 3. Rectifiers and rectification mechanisms. Adapted from references 10, 43, and 54 to 58.

Systems in which the rectification of current happens through cobaltocene appeared in 2006 with Liu *et al.*⁸⁴ suggesting that metallocenes should make excellent molecular diodes. In the same year Metzger *et al.*⁸⁵ presented a system in which ferrocene serves as the donor and perylene-bisimide is the acceptor; rectification ratios (*RR*) of 14 to 28 were observed between ± 1 V for up to 40 cycles. Years later molecular transistors based on self-assembled monolayers of ferrocene chemically bound to a flat Au electrode and a Au nanoparticle as drain electrodes were developed by Richter and collaborators.⁸⁶ Measured *I/V* curves shifted from symmetric to strongly rectifying, depending on the gate voltage range. The Lee group⁸⁷ investigated the use of redox-induced properties on ferrocene-alkanethiolate systems using a conducting polymer-interlayer device structure. They observed asymmetric behavior arising from the ferrocene moiety. This system showed current decreases associated with increasing temperatures (> 220 K) and large applied positive bias (> 0.6 V). Impressive results were obtained by Nijhuis *et al.*,⁸⁸ both by relating the above-described temperature control of electron transfer to molecular levels or Coulomb repulsion,^{88a} as well as by developing bis-ferrocene systems^{88b} that use sequential tunnelling to yield very high rectification ratios. Terpyridines were used in a $[\text{Mn}^{\text{II}}(\text{terpy-O}(\text{CH}_2)_6\text{-SAC}_2)]^{2+}$ system studied by van der Zant *et al.*,⁸⁹ which demonstrated an electrically controlled high-spin/low-spin transition between $^{55}\text{Mn}^{\text{II}}$ ($S = 5/2$) and $^{55}\text{Mn}^{\text{II}}$ ($S = 1/2$) by adjusting the gate-voltage. The terpyridine moiety gets reduced, thus altering the ligand-field around the metal.

Surfactants and their ordered monolayer films

As previously mentioned, monolayers and multilayers have been used with remarkable success in the preparation of molecular rectifiers. These films are often obtained via isothermal compression of surfactants or surface-acting agents. These molecules contain a polar water-soluble portion—the hydrophilic headgroup—along with an apolar water-insoluble—thus hydrophobic—counterpart (Figure 4a). This amphiphilic nature

leads to competing forces acting to yield an energetically favorable conformation when the surfactant is in contact with a fluid surface such as water. Surfactants tend to assemble in aggregate structures with two possible thermodynamic extremes associated with their dominant hydrophobic or hydrophilic nature. If the hydrophilic behavior prevails, spontaneous formation of molecular aggregates such as micelles takes place when a critical concentration is reached. On the other hand, if the hydrophobic portion of the surfactant predominates, a two-dimensional film will be formed at the air/water interface.

Pockels-Langmuir and Langmuir-Blodgett monolayers

Assuming the thickness of the film to be similar to that of a single molecule, the resulting film is called a Pockels-Langmuir⁹⁰ (PL) monolayer and is shown in Figure 4b. The usual technique to evaluate the properties of these monolayers, as well as their associated multilayers, is a 2D compression isotherm⁹¹ that plots the variability of surface pressure vs. average molecular area (π vs. A isotherms) at constant temperature and variable film area comprised between the movable barriers of a trough.⁹² The surface pressure is defined as $\pi = \gamma_0 - \gamma$ where γ_0 the surface tension of the aqueous subphase and γ is the surfactant-modified surface tension. The average area occupied per surfactant molecule is obtained as a function of its concentration and the enclosed area between the trough barriers.^{93, 94} A schematic compression isotherm is shown in Figure 4c, from which information relative to the organization, orientation, and conformation of the monolayer can be assessed. Information on the limiting area per molecule, the area, pressure, and mechanism of monolayer collapse can be determined.⁹⁵ Additionally, analysis of distinct regions of the compression isotherm lead to information on 2D crystalline, condensed isotropic, or anisotropic liquid phases⁹⁶ with different degrees of packing, molecular tilt and twist angles, rotational freedom, and defects.⁹⁷ Once a suitable PL monolayer is obtained, it can be transferred retaining molecular order and patterns onto solid substrates using Langmuir-Blodgett⁹⁸ (LB) deposition Figure 4d. If carefully performed, the PL monolayer can be transferred reproducibly as an LB monolayer on solid substrates. As such, the transfer ratio, given by the area occupied by the monolayer on water vs. the area of the transferred monolayer on solid, can be measured accurately, and should approach unity. It is accepted that a short distance between the molecules of a monolayer will be necessary for electron or charge transfer process that is at the very center of molecular rectification.⁹⁹ Compared to self-assembly where only one value of area per molecule can be attained, LB deposition leads to a more precise control of molecular order and packing.

Deposition onto solid surfaces can be done at any point on the 2D compression isotherm and enable high packing densities of up to 20 Å² per molecule for regular organic surfactants, even in presence of transition metals.¹⁰⁰ This average area corresponds to an approximate molecular distance of 4.5 Å between surfactants, thus well within the intermolecular distance observed by X-ray diffraction of single crystals.¹⁰¹ As such, the use of LB monolayers

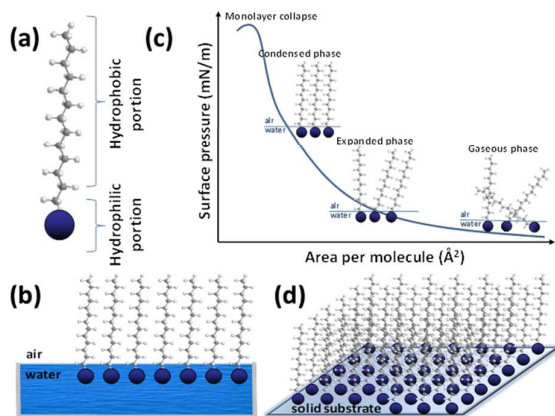


Figure 4. Surfactants and monolayers: (a) scheme of a surfactant, (b) plot of surface pressure vs. average area per molecule, (c) ordered Pockels-Langmuir film at the air/water interface, (d) Langmuir-Blodgett film at the air/solid interface

for molecular rectification allows for the formation of uniform and scalable films with excellent control over packing and ordering, and offers an alternative to single-molecule and self-assembled methods.

Monolayer characterization

The resulting LB film can be further evaluated by several complimentary interface-dedicated methods. The most relevant microscopic methods include Brewster angle and atomic force microscopies, while infrared reflection absorption figures among the chief spectroscopic approaches. Brewster angle microscopy (BAM)^{102, 103} is a technique that is carried out simultaneously with the LB experiment to visualize various changes occurring on the surface of the subphase. This technique uses the principle of zero-reflectance of the air/water interface for a vertically polarized light at an angle of incidence θ called the Brewster angle. This angle depends on the refractive indices of the materials in the system as it satisfies the relation, $\tan\theta = n_{\text{subphase}}/n_{\text{air}}$, with n being the refractive index. When a monolayer with different refractive index is spread on a given interface, some change in reflectivity will occur. The reflected light can then be used to form a high contrast image of the layer. Atomic force microscopy¹⁰⁴⁻¹⁰⁶ (AFM) provides information regarding the surface features of the films. The probe, connected to the end of a cantilever, smoothly scans the surface of the sample creating a data map with information regarding the surface morphology and roughness, as well as the thickness of mono and multilayer LB films on mica, quartz, and gold. Infrared reflection absorption spectroscopy¹⁰⁷ (IRRAS) is an invaluable method in the characterization of LB films deposited on dielectric solids. The resulting spectrum depends on the optical constants of the film and the substrate, the angle of incidence, as well as the p - and s - polarized components of the incident IR radiation. The resulting spectrum resembles that of a regular IR experiment, and enables information about functional groups and comparisons between the nature of the material to be deposited as a LB film as bulk material and as a thin film. Contact angle measurements are also done to establish the hydrophilicity or the hydrophobicity of the deposited LB films. The contact angle is the angle between the solid surface and the liquid/vapor. A drop with poor wetting and adhesiveness and a low solid surface free energy will be hydrophobic, and yield a contact angle greater than 90° whereas a very small contact angle is associated with hydrophilicity, as a result of better wetting, better adhesiveness, and higher surface energy.

Metal-containing surfactants

The combination of the aforementioned amphiphilic behavior with the well understood, controllable, and tunable properties of transition metal complexes leads to new materials that exhibit interfacial organization, along with variable geometric, charge, redox, optical, and magnetic properties; the notion of controlled and reversible redox behaviour is particularly relevant. The design of metal-containing surfactants —metallo-surfactants— involves the

synthesis of amphiphilic molecules capable of incorporating the metal ion to the polar headgroup by means of chemical bonding. The understanding of the cooperativity between transition metal ions and amphiphilic organic scaffolds in metallosurfactants has become desirable due to its potential relevance toward high-end technological applications, many of them within the field of molecular electronics. On the one hand, the metal ion can either exhibit preferential geometries that favor octahedral or tetrahedral headgroups, or foster distinctive protonation status. On the other hand, the denticity (number of donor atoms) and the rigidity of the ligand also play an important role. Therefore, the final topology and properties of a given metallosurfactant are dictated by the nature of both the metal ion and the amphiphilic ligand influencing the properties of the resulting films.

We started the study of responsive metal-containing surfactants in the mid-2000s working primarily on the coordination chemistry aspects of these materials. We favored asymmetric $[\text{ML}_2]^{0/+}$ species containing Fe^{III} ,¹⁰⁸ Co^{III} and Co^{II} ,¹⁰⁹ Ni^{II} , Cu^{II} , and Zn^{II} ¹¹⁰ ions coordinated to chelating headgroups containing pyridine, amine/imine, and phenolate donors (**Figure 5**). These complexes contain an asymmetric $[\text{N}_{\text{py}}\text{N}_{\text{am/im}}\text{O}_{\text{phen}}]$ chelating headgroup present in the amphiphiles, but omit the hydrophobic alkyl chain. They serve as archetypical models to understand complex coordination modes, spectral, redox properties, and protonation preferences of often non-crystalline surfactants with potential use in redox-responsive LB films. This specific environment with asymmetric donors was pivotal as a proof-of-concept approach because the presence of different metal centers led to both structural and electronic effects that determine the preferential

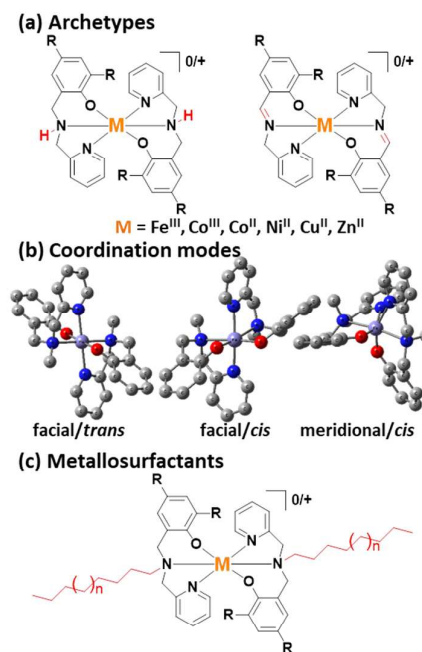


Figure 5. Early pseudo-octahedral $[\text{N}_{\text{py}}\text{N}_{\text{am}}\text{O}_{\text{phe}}]$ systems: (a) archetypical modelling, (b) possible coordination modes of tridentate asymmetric ligands, and (c) example of metallosurfactants.

geometry adopted by the resulting complexes.^{111, 112} We observed that equivalently asymmetric [NN'O] chelates containing amines and imines are bound to a metal ion, the ligand rigidity of imines precedes electronic configuration and imposes a meridional coordination. However, electronic configuration determines the final coordination mode of flexible amines: facial coordination is always favored, but configuration dictates the preferential *cis*- or *trans*- orientation of equivalent phenolates, pyridines, and amines in vicinal ligands. The Fe^{III} ion with a ⁵3d⁵ configuration led to *cis*-arrangements of the phenolates while ⁵3d⁶ Co^{III} and ⁵3d⁷ Co^{II} ions support *trans*-orientation of those groups. Lacking ligand field stabilization energy, the 3d¹⁰ ions Zn^{II} or Ga^{III} show no preference.

Through this approach, we established the value of archetypical modelling as an experimental tool to understand structurally complex amorphous and oily materials, and to guide the design of metal-containing surfactants as precursors for redox-responsive LB films.¹¹³ After building a good understanding on the coordination modes of archetypes, we moved towards understanding the distinctions between organic surfactants and metallosurfactants on the compression and collapse of films. We have demonstrated that two similar Co^{II/III}-containing surfactants differing only by the presence of octadecyl- or nonyloxybenzyl-functionalities incorporated to the secondary amine of the NN'O chelates exhibit amphiphilic properties. The species organize well at the air/water and air/solid interface, but exhibit dissimilar collapse mechanisms at either isothermal constant pressure or constant area.^{109, 114} These studies pioneered the use of BAM methodology for metallosurfactants. The coordination modes and interfacial behavior of 3d⁵⁻⁸ and 3d¹⁰ ions being better understood, we moved onto the investigation of the subtle equilibrium between amphiphilic and redox properties in cationic Cu^{II}-containing surfactants. The redox reversibility of these species posed a particular challenge¹¹⁵ associated with coordination changes upon reduction from five-coordinate 3d⁹ Cu^{II} to four-coordinate 3d¹⁰. However, these studies expanded on BAM and led to the unprecedented use of IRRAS methods on the characterization of metallosurfactant PL and LB films.¹⁰³ In particular, BAM allowed for a detailed examination of PL film patterning at the air/water interface and the association of these patterns with subphase modifications.^{100, 116} These modifications later led to studies on how these species influence the alignment of nematic liquid crystals,¹¹⁷ as well as their own liquid crystalline behavior.¹¹⁸

Archetypes for five-coordinate Fe^{III} surfactants

Due to superior redox-reversibility, Fe^{III}-containing complexes and surfactants display particular relevance. Contemporaneous to the study of surfactants based on asymmetric [NN'O] chelators described above, we were investigating the redox and electronic behavior of five-coordinate ⁵3d⁵ Fe^{III} complexes bound to phenolate-rich [N₂O₃] environments. These species were inspired by the active site of Tyrosine Hydroxylase,¹¹⁹ which catalyzes the hydroxylation of the amino acid L-tyrosine to L-3,4-dihydroxyphenylalanine (L-DOPA) via unique redox and radical

mechanisms. Two papers paved the way to the development of functional materials intended for molecular electronics. The first study on five-coordinate Fe^{III} and Ga^{III} complexes involved the nature of structural and electronic changes associated with redox-triggered ground states associated with either the metal ion or the multiple phenolate groups in asymmetric environments.¹²⁰ The new pentadentate [N₂O₃] ligand *N,N,N'*-tris-(3,5-di-*tert*-butyl-2-hydroxybenzyl)-benzene-1,2-diamine, **H₃L¹** was synthesized and treated with Fe^{III} and Ga^{III} salts to afford the neutral species [Fe^{III}L¹] and [Ga^{III}L¹], **Figure 6a-b**. Each of the three phenolates can be oxidized and support the reversible formation of phenoxyl radicals. The complexes were characterized *via* elemental analysis, ESI spectrometry, as well as crystallographic, electrochemical, spectro-electrochemical, EPR, and DFT methods. The Fe^{III} ion is surrounded by three phenolate oxygen atoms and two amine nitrogen atoms of (L¹)³⁻. Two oxygen and one nitrogen atoms form a trigonal plane around the metal center, whereas the remaining oxygen and nitrogen atoms occupy the apical positions of the distorted trigonal bipyramid with τ index of 0.53.¹²¹ The bond distances for Fe-N and Fe-O are well within the expected range.^{122, 123} The molecular structure of [Ga^{III}L] was also determined, and served as an important model to ascertain the metal- and ligand-based redox

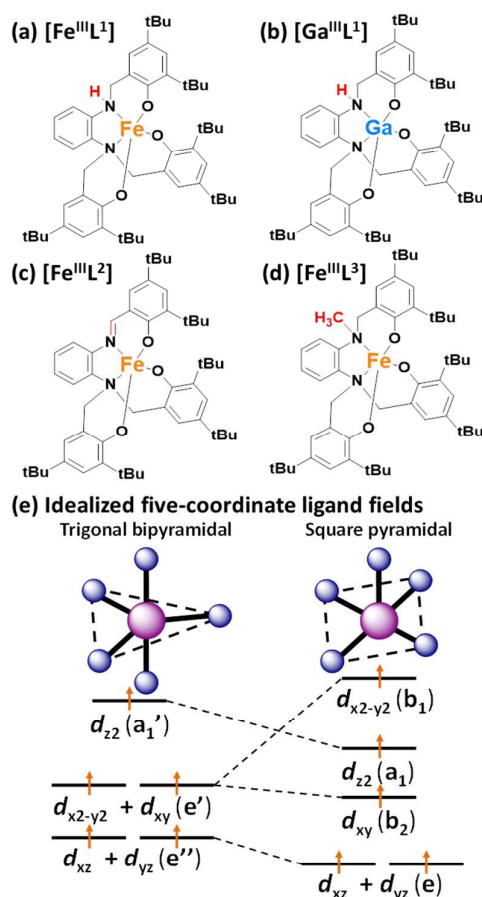


Figure 6. Five-coordinate ⁵Fe^{III} and Ga^{III} archetypes, geometries, and ligand fields.

potentials. The cyclic voltammogram of $[\text{Fe}^{\text{III}}\text{L}^1]$ shows a $1e^-$ process at $-1.44 \text{ V}_{\text{Fc}^+/\text{Fc}}$ assigned to the $\text{Fe}^{\text{III}}/\text{Fe}^{\text{II}}$ redox couple. No comparable process was found for the Ga^{III} species. Three phenolate-to-phenoxy radical processes were observed at 0.51, 0.77 and 0.99 V. The metal and first ligand processes were cycled 20 times simulating a redox switching mechanism necessary for electron transfer, with no detection of decay in current amplitude. These results are shown in **Figure 7**, along with comparisons of the redox behaviour of five-coordinate Fe^{III} surfactants discussed in the next section.

Species $[\text{Fe}^{\text{III}}\text{L}^1]$ shows an EPR signal at $g = 4.26$, and confirms an expected high spin configuration, where a single electron occupies each of the five 3d-based MOs in increasing order: $e'' (d_{xz}^1, d_{yz}^1) e' (d_{x^2-y^2}^1, d_{xy}^1) a_1' (d_{z^2}^1)$. Therefore the lowest lying set of orbitals is described as an e'' set. For later systems we also observed a square pyramidal symmetry with idealized $e (d_{xz}^1 + d_{yz}^1) b_2 (d_{xy}^1) a_1 (d_{z^2}^1) b_1 (d_{x^2-y^2}^1)$ configuration (see **Figure 6e**). A phenoxy-related signal at $g = 2.00$ was also observed. Interestingly, a slow oxygen-dependent conversion of the secondary amine group of the ligand to the corresponding imine (azomethine) was observed for both Fe^{III} and Ga^{III} complexes. These imines lose two hydrogen atoms and form a new C=N group but do not change the total oxidation state of the species.¹²⁴ The second account¹²⁵ led to the investigation of imine-bearing $[\text{Fe}^{\text{III}}\text{L}^2]$ and methylated $[\text{Fe}^{\text{III}}\text{L}^3]$ (**Figure 6c-d**), in which a similar low-symmetry ligand field is purposefully enforced around the $3d^5$ metal ion via $[\text{N}_2\text{O}_3]$ ligands. The new ligands H_3L^2 and H_3L^3 are structurally related to the above-described H_3L^1 , and differ on the respective presence of an imine or methylamine group that precludes amine conversion to imine. Both species display four redox-accessible ground states associated with $[\text{Fe}^{\text{III}}\text{L}^i]^{0/+}$, $[\text{Fe}^{\text{III}}\text{L}^i]^+$, $[\text{Fe}^{\text{III}}\text{L}^i]^{2+}$, and $[\text{Fe}^{\text{III}}\text{L}^i]^{3+}$, and the sequence by which each of the phenolate rings is oxidized depends on steric and electronic factors

associated with the azomethine/methylamine groups. While both species display the $\text{Fe}^{\text{III}}/\text{Fe}^{\text{II}}$ couple at about $-1.50 \text{ V}_{\text{Fc}^+/\text{Fc}}$ the imine-bearing $[\text{Fe}^{\text{III}}\text{L}^2]$ shows ligand-based processes at 0.55 and 0.73 $\text{V}_{\text{Fc}^+/\text{Fc}}$ and the methylamine-bearing $[\text{Fe}^{\text{III}}\text{L}^3]$ displays values of 0.48 and 0.75 $\text{V}_{\text{Fc}^+/\text{Fc}}$. Interestingly, the third ligand-centered process was not observed for the former species, and appeared as an irreversible process at 1.09 $\text{V}_{\text{Fc}^+/\text{Fc}}$ for the latter. These species withstand well over thirty redox cycles at 150 mV/s without noticeable decomposition. The electronic behavior of $[\text{Fe}^{\text{III}}\text{L}^2]$ and $[\text{Fe}^{\text{III}}\text{L}^3]$ in dichloromethane was compared to that of their oxidized counterparts and evidence the disappearance of phenolate-to-metal charge transfer (CT) processes seen around 450 nm upon bulk electrolysis at -78°C . This CT band involves in- and out-of-plane $p\pi_{\text{phenolate}} \rightarrow d\sigma_{\text{Fe}}^*$ and $p\pi_{\text{phenolate}} \rightarrow d\pi_{\text{Fe}}^*$ transitions and serves as a spectroscopic handle indicative of the transformation of one phenolate into a phenoxy radical. A new band attributed to a phenolate-to-phenoxy interligand CT also appears at $\sim 750 \text{ nm}$. This transformation is confirmed by the disappearance of an EPR peak at $g \approx 4.3$ upon oxidation. That peak is similar to the one observed for $[\text{Fe}^{\text{III}}\text{L}^1]$ and diagnostic of a five-coordinate $^{\text{HS}}\text{Fe}^{\text{III}}$ in largely anisotropic ligand fields. This is consistent with the existence of an antiferromagnetically coupled $[\text{Fe}^{\text{III}}\text{L}^i]$ species with an integer spin $S = 4/2$. Because the timescale of the bulk electrolysis experiment aiming to the doubly and triply oxidized products led to mixtures, the sequential oxidations $[\text{Fe}^{\text{III}}\text{L}^i] \rightarrow [\text{Fe}^{\text{III}}\text{L}^i]^+ \rightarrow [\text{Fe}^{\text{III}}\text{L}^i]^{2+}$ were investigated by DFT methodology. The results show that subtle structural changes in $[\text{Fe}^{\text{III}}\text{L}^2]$ and $[\text{Fe}^{\text{III}}\text{L}^3]$ suffice to trigger distinct phenolate oxidation sequences. While the imine-containing $[\text{Fe}^{\text{III}}(\text{L}^2)]^+$ and $[\text{Fe}^{\text{III}}(\text{L}^2)]^{2+}$ bear the first and second phenoxy radical in the vicinal phenolates that originate from the tertiary amine nitrogen, $[\text{Fe}^{\text{III}}(\text{L}^3)]^+$ will have its first oxidation at the methylamine group side. Only then, one of the phenolates tethered to the tertiary nitrogen will be oxidized to form $[\text{Fe}^{\text{III}}(\text{L}^3)]^{2+}$. This observation allowed us to assign individual redox loci within each of these compounds and to move one step further towards the development of candidates for molecular rectification. In order to study these species in electrode|molecule|electrode assemblies, organization and alignment in LB monolayers was necessary.

Rectification with five-coordinate Fe^{III} surfactants

Moving from biomodeling to electronic structure to functional materials, these species were altered with appended alkoxy chains to the phenylene ring aiming to merge the observed redox response to amphiphilic behavior and film deposition. This modification led to the design of redox-responsive metallosurfactants. We have published several comprehensive studies investigating (i) the development of metallosurfactant-based assemblies, (ii) the correlation of electronic structure and redox behavior with the mechanisms of molecular rectification, (iii) the confirmation of rectifying behavior with independent methodology, (iv) the furthering of metallosurfactant systems in which the $^{\text{HS}}\text{Fe}^{\text{III}}$ ion is in asymmetric ligand fields, and (v) the *in situ* spectroelectrochemical

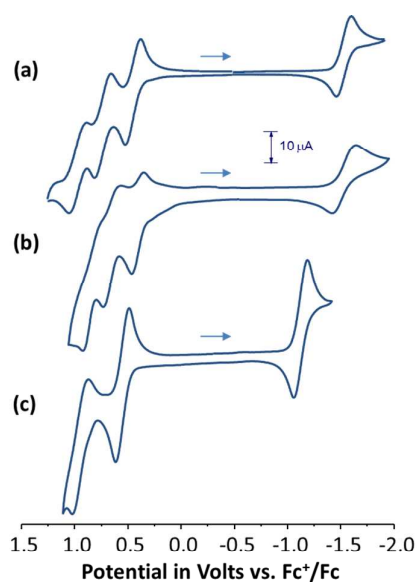


Figure 7. Selected redox responses for (a) $[\text{Fe}^{\text{III}}\text{L}^1]$, (b) $[\text{Fe}^{\text{III}}\text{L}^4]$, and (c) $[\text{Fe}^{\text{III}}\text{L}^6\text{Cl}]$.

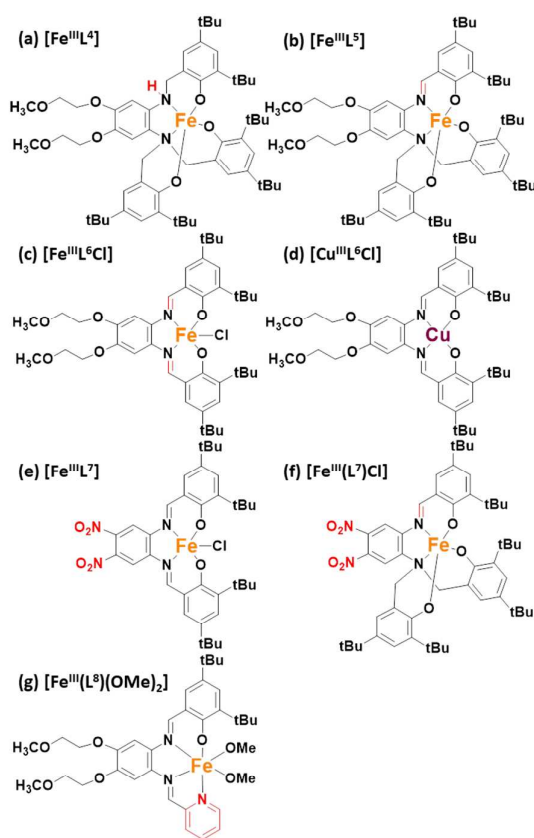


Figure 8. Currently studied five-coordinate $^{55}\text{Fe}^{\text{III}}$ molecular rectifiers and Cu^{III} insulator.

interrogation of molecular orientation change in molecular LB Films on gold electrode surfaces.

In 2013 we published an account¹²⁶ on a new metallosurfactant [$^{55}\text{Fe}^{\text{III}}\text{L}^4$] (**Figure 8a**) based on the redox-active [N_2O_3] environment described in the previous section.

The complex displays phenylenediamino-metal and phenolate moieties that can act, respectively, as electron acceptors and donors. The $\text{Fe}^{\text{III}}/\text{Fe}^{\text{II}}$ redox couple appears as a cathodic process at $-1.49 \text{ V}_{\text{Fc}^+/ \text{Fc}}$ whereas three consecutive phenolate/phenoxyl processes were seen at 0.43 , 0.69 , and $0.90 \text{ V}_{\text{Fc}^+/ \text{Fc}}$ (**Figure 7b**). Aiming to build nanoscale devices based on LB films of [$\text{Fe}^{\text{III}}\text{L}^4$], we evaluated its air/water interfacial properties using isothermal compression and BAM, assessing the average area per molecule, collapse pressure of the monolayers, and film homogeneity (**Figure 9a-b**). The formation of a homogeneous PL monolayer was observed at surface pressures of around $10\text{--}20 \text{ mN/m}$, followed by a phase rearrangement between 25 and 35 mN/m . The homogeneity of the film remained unaltered until ridge formation indicative of collapse appeared at 63 mN/m . The simplest model for molecular arrangement at the air/water interface suggests the methoxyethane moiety submerged in water, whereas the hydrophobic iron/phenolate core remains at the air subphase. Thus, the approximate area occupied by this core is *ca.* 200 \AA^2 for optimal

packing. Indeed, the critical areas towards the end of the phase transition at 35 mN/m yielded a tightly packed film with optimized topology. The LB films were deposited either as monolayers or multilayers onto glass or mica substrates and studied by UV-visible, IR, IRRAS, contact angle, and AFM. The general $\pi\text{-}\pi^*$ and LMCT features present in the solution spectrum of [$\text{Fe}^{\text{III}}\text{L}^4$] were maintained, but an intensification of the N- Fe^{III} LMCT band at 330 nm , was observed along with the hypsochromic shift of the in- and out-of-the-plane $\text{PhO}^-\text{Fe}^{\text{III}}$ band at 470 nm , and a new phenolate-to-azomethine CT band at 400 nm was associated with amine/imine conversion of the ligand that takes place at the air/water interface. The conversion of [$\text{Fe}^{\text{III}}\text{L}^4$] into an imine species [$\text{Fe}^{\text{III}}\text{L}^5$] (**Figure 8b**) was further probed by IRRAS, (**Figure 9c**) with a new $\text{C}=\text{N}$ peak appearing at 1583 cm^{-1} . In the previously studied [$\text{Fe}^{\text{III}}\text{L}^2$] system the imine ligands show slightly less positive potentials for the phenolate/phenoxyl processes, indicating a decrease in the HOMO-LUMO gap. Further examination of the CH_3 peaks present in the IRRAS spectra from 2954 cm^{-1} in the bulk sample to 2962 cm^{-1} in the film corroborated with a well-packed film where the $\text{Fe}/\text{phenolate}$ moiety points outwards. Contact angle measurements of the film yielded a value of 85.30° , compared to 7.45° for the substrate alone, thus confirming the hydrophobic nature of the resulting [$\text{Fe}^{\text{III}}\text{L}^5$] film. The morphology of the LB monolayer was measured by AFM on mica at surface pressures of 10 , 25 , 30 , 33 , and 40 mN/m . While pinholes were detected at low surface pressures, the monolayer was smooth at 33 mN/m . The thickness of a single monolayer was determined by AFM on quartz substrates containing between 1 to 15 layers by blade-scratching the film (**Figure 10a-b**). A linear relationship between thickness and number of layers indicated homogeneous film deposition in which each layer was $19 \pm 2 \text{ \AA}$ thick. The result is in excellent agreement with the estimated $16\text{--}17 \text{ \AA}$ for a monolayer composed by well-packed molecules where the alkoxy chains contact the solid substrate and the *tert*-butyl rich $\text{Fe}/\text{phenolate}$ moiety points outwards at the air/solid interface. In order to build $\text{Au}|\text{LB}[\text{Fe}^{\text{III}}\text{L}^5]|\text{Au}$ assemblies, a PL monolayer was transferred at 33 mN/m onto a gold-coated mica substrate. In order to build $\text{Au}|\text{LB}[\text{Fe}^{\text{III}}\text{L}^5]|\text{Au}$ assemblies, a PL monolayer was transferred at 33 mN/m onto a pre-cleaned gold-coated mica substrate, yielding a defect free LB film. After being vacuum-dried, this film received a top “cold gold” electrode in an EffaCoater gold sputter using shadow masking and argon as the carrier. Three assemblies with 16 devices each (**Figure 10c-d**, 48 devices) were fabricated and the current–potential (I - V) characteristics were reproducibly measured at ambient conditions in four to five devices per assembly using a probe station (Signatone S-1160) coupled to a parameter analyzer (Keithley 4200).¹²⁶ As expected,^{55,56} some devices were short-circuited due to monolayer defects. In each of the well-formed devices I/V measurements a higher current is observed in the third quadrant than in the first quadrant. This asymmetric I/V characteristic of a sharp negative response and a negligible positive response is indicative of rectification behavior, as shown in **Figure 11a**. The rectification ratio ($RR = [I \text{ at } -V_0 / I \text{ at } +V_0]$)⁵³ for the monolayer of [$\text{Fe}^{\text{III}}\text{L}^5$] varies from 4.5 to 12 between -2 to $+2 \text{ V}$ and from 2.9 to 37 between -4 to $+4 \text{ V}$,

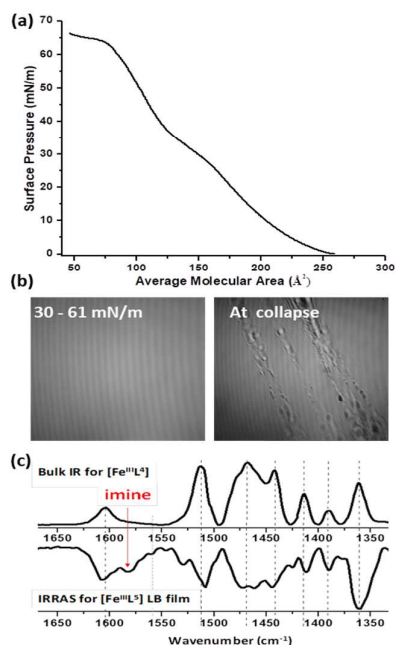


Figure 9. Examples of (a) Isothermal compression of an LB monolayer for $[\text{Fe}^{\text{III}}\text{L}^4]$, (b) BAM microscopy showing collapse, and (c) comparison between the IR of $[\text{Fe}^{\text{III}}\text{L}^4]$ and the IRRAS spectrum for the LB film of imine-containing $[\text{Fe}^{\text{III}}\text{L}^5]$.

respectively. Reversing the drain and the source contacts demonstrated retention of the rectification behavior. Although the rectifying behavior was observed, it was only partially understood and we assumed contributions from asymmetrical and unimolecular mechanisms in which possible $[\text{DA}]$ and $[\text{D}^+\text{A}^-]$ states may be proposed. Considering that (i) the reduction of Fe^{III} to Fe^{II} and the oxidation from phenolate to phenoxyl were observed, while (ii) neither reduced anionic radicals nor the $\text{Fe}^{\text{III}}/\text{Fe}^{\text{IV}}$ oxidation were observed, we proposed the involvement of the $\text{Au}|\text{PhO}^- - \text{Fe}^{\text{III}}|\text{Au}$ and $\text{Au}|\text{PhO}^- - \text{Fe}^{\text{II}}|\text{Au}$ states, where the HOMO is ligand-based and the LUMO is metal-centered. However, the LUMOs are higher in energy and the metal-based MOs are partially occupied SOMOs of e'' , e' , and a_1' symmetry in a trigonal bipyramidal $3d^5$ HSFe^{III} species. This observation compelled us to further study this phenomenon using a synthetic coordination chemical approach.¹²⁷ In 2014 we evaluated the rectification response of two new metallosurfactants, the $\text{HS}3d^5$ $[\text{Fe}^{\text{III}}(\text{L}^6)\text{Cl}]$ ($S = 5/2$) and the $3d^9$ $[\text{Cu}^{\text{II}}\text{L}^6]$ ($S = 1/2$) based on a new $[\text{N}_2\text{O}_2]$ ligand (Figure 8c-d), aiming to correlate electronic structure with the mechanisms that determine molecular rectification in coordination complexes. We hypothesized that $[\text{HSFe}^{\text{III}}(\text{L}^6)\text{Cl}]$, with a low-energy e'' (d_{xz}^1, d_{yz}^1) set, would be prone to accept an electron and enable current rectification. The $[\text{Cu}^{\text{II}}\text{L}^6]$ would display a single high-energy SOMO described as $3d_{x^2-y^2}$ and likely not available for electron transfer. Indeed, the $\text{Fe}^{\text{III}}/\text{Fe}^{\text{II}}$ couple appeared at $-1.02 V_{\text{Fc}^+/ \text{Fc}^-}$, whereas the $\text{Cu}^{\text{II}}/\text{Cu}^{\text{I}}$ reduction appears at $-1.85 V_{\text{Fc}^+/ \text{Fc}^-}$. Metallosurfactants $[\text{HSFe}^{\text{III}}(\text{L}^6)\text{Cl}]$ and $[\text{Cu}^{\text{II}}\text{L}^6]$ formed homogeneous PL films with respective constant collapse pressures of 40 and 30 mN/m and critical average molecular areas of 71 and

$79 \text{ \AA}^2/\text{molecule}$. These films enabled the fabrication of $\text{Au}|\text{LB}|\text{Au}$ assemblies, each with 16 devices, as previously described. An average of 30% of devices showed rectification in each of these assemblies. Devices of $\text{Au}|\text{LB}[\text{Fe}^{\text{III}}(\text{L}^6)\text{Cl}]|\text{Au}$ showed asymmetric response with elevated electrical current in the negative quadrant and negligible response in the positive quadrant, as indicative of rectifying behavior (Figure 11c). The rectification ratio ($RR = |I \text{ at } -V_0|/I \text{ at } +V_0$) ranges from 4 to 29 between -2 to $+2$ V and from 2 to 31 between -4 to $+4$ V, thus comparable to the previous example. Remarkably, $\text{Au}|\text{LB}[\text{Cu}^{\text{II}}\text{L}^6]|\text{Au}$ yielded flat I/V curves characteristic of non-rectifying devices (Figure 11d). These results agree with our hypothesis and require that the Fermi levels (E_F) of the electrodes must be compatible with the energies of the SOMOs in order to facilitate resonant tunneling via different redox states of a given species. The E_F for gold electrodes is 5.1 eV below the vacuum,¹²⁸ and electron transfer will be favored by the systems with the best match between E_F and HOMO/LUMO or more properly here, HOMO/SOMO energies. $[\text{Fe}^{\text{III}}(\text{L}^6)\text{Cl}]$ has a smaller ΔE ($E_{\text{pa1}} - E_{\text{pc1}}$) of 1.78 V (Figure 7c) associated with a narrower HOMO-LUMO gap, while $[\text{Cu}^{\text{II}}\text{L}^6]$ yields a ΔE of 2.39 V. Using the equations $V_a = 4.7\text{eV} + E_{1/2}^{\text{red}}(\text{SCE})$ and $V_i = 4.7\text{eV} + (1.7) E_{1/2}^{\text{ox}}(\text{SCE})$,¹²⁹⁻¹³² the experimental molecular redox potentials were converted to comparable solid-state potentials. The $[\text{Fe}^{\text{III}}(\text{L}^6)\text{Cl}]$ shows the first metal-centered SOMO at -4.1 eV, while that of $[\text{Cu}^{\text{II}}\text{L}^6]$ is found at -3.2 eV. Similarly, the first ligand-centered HOMOs are respectively found at -6.5 and -6.1 eV. As such, the model depicted in Figure 12a, shows the gold Fermi levels at *ca.* 1.0 eV below the lowest Fe-based SOMO and 2.0 eV below the lowest Cu-based SOMO. As predicted using ligand field arguments, DFT calculations confirm those MOs as a linear combination of $d_{xz} + d_{yz}$ (z -axis along the Fe-Cl bond) for $[\text{Fe}^{\text{III}}(\text{L}^6)\text{Cl}]$ and as the energetically mismatched $d_{x^2-y^2}$ orbital for $[\text{Cu}^{\text{II}}\text{L}^6]$.

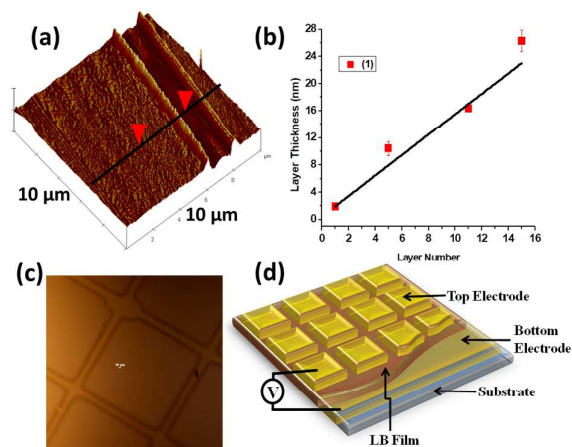


Figure 10. Surface morphology and assembly fabrication: (a) AFM of an LB film for $[\text{Fe}^{\text{III}}\text{L}^5]$ on quartz used in height measurements to determine monolayer thickness, (b) thickness (nm) vs. number of layers plot from mono to 15 layers; (c) an optical micrograph of the $\text{Au}|\text{LB}|\text{Au}$ assembly; (d) schematic view of the assembly layout.

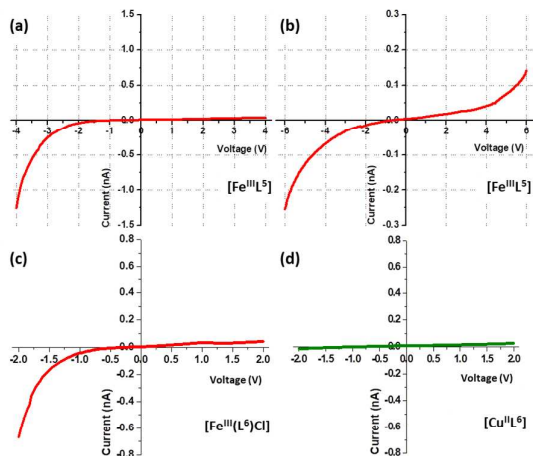


Figure 11. Example of experimental I/V curves showing (a) rectification and (b) symmetrical response upon repeated cycles for $[\text{Fe}^{\text{III}}\text{L}^5]$, (c) rectification for $[\text{Fe}^{\text{III}}(\text{L}^6)\text{Cl}]$, and (d) insulation for $[\text{Cu}^{\text{II}}\text{L}^6]$.

The ligand-based HOMOs were found 1.4 eV below the Au E_F and were initially considered as not involved in the rectification process. We called this SOMO only process as asymmetric.^{70, 84} As such, rectification seems to involve a mechanism partially described as $[\text{Fe}^{\text{III}}\text{L}^5] (d_{xz}^1 + d_{yz}^1) \rightleftharpoons [\text{Fe}^{\text{II}}\text{L}^5]^- (d_{xz}^2 + d_{yz}^1) \longleftrightarrow [\text{Fe}^{\text{II}}\text{L}^5]^- (d_{xz}^1 + d_{yz}^2)$. Because the films are physisorbed between two identical electrodes, we discard a Schottky mechanism^{56, 58} and favor an asymmetrical mechanism. Unimolecular mechanisms could be supported in these molecules if the involved MOs were to display favorable energies. As such, in 2016 we conducted a systematic evaluation¹³³ of the possible pathways that lead to rectification by comparing the SOMO-Fermi-HOMO energy gap in four $^{\text{H}}\text{Fe}^{\text{III}}$ complexes with $[\text{N}_2\text{O}_2\text{Cl}]$ and $[\text{N}_2\text{O}_3]$ coordination spheres, namely the just described $[\text{Fe}^{\text{III}}\text{L}^5]$ and $[\text{Fe}^{\text{III}}(\text{L}^6)\text{Cl}]$ along with the nitro-substituted $[\text{Fe}^{\text{III}}\text{L}^7]$ and $[\text{Fe}^{\text{III}}(\text{L}^7)\text{Cl}]$ (Figure 8e-f). The methodology was similar to that just described above, measuring experimentally the redox potentials in volts, and converting those into solid state eV values, then using DFT calculations based on X-ray structures to assess the nature of the HOMO/SOMO orbitals. The presence of an apical chlorido or phenolato ligand, plays a crucial role, and while $[\text{Fe}^{\text{III}}(\text{L}^6)\text{Cl}]$ and $[\text{Fe}^{\text{III}}(\text{L}^7)\text{Cl}]$ support an asymmetric mechanism, $[\text{Fe}^{\text{III}}\text{L}^5]$ and $[\text{Fe}^{\text{III}}\text{L}^7]$ could be closer to unimolecular mechanisms. These results allowed us to postulate that SOMO-HOMO modulation can be attained if an appropriate apical ligand and/or substituent framework is/are present. On the one hand, if the SOMO energy is close to the E_F of the electrodes, asymmetric rectification will be favored and HOMO participation is likely excluded. On the other hand, approaching the energy of the HOMO to that of the electrode E_F may favor rectification towards a unimolecular pathway. As such, this MO modulation to match the Fermi levels of the electrodes expands the very concept of a molecular rectifier and allows for a more rational design of future systems. In 2016 the Metzger group measured and confirmed the rectifying behavior of $[\text{H}^{\text{S}}\text{Fe}^{\text{III}}(\text{L}^6)\text{Cl}]$ using dissimilar electrodes.¹³⁴

This new methodology played an important role in promoting an independent verification of the rectification observed in five-coordinate $^{\text{H}}\text{Fe}^{\text{III}}$ surfactants. In order to proceed, an LB monolayer of $[\text{Fe}^{\text{III}}(\text{L}^6)\text{Cl}]$ was deposited on a Au electrode and topped with a soft contact of gallium indium eutectic,^{70b} or EGaIn/Ga₂O₃|LB|Au assembly. When scanned from 0 to -1.5 V, 90% of the sandwiches remained stable, while scanning from 0 to +1.5 V only 10% remained stable. For the scan range of ± 0.7 V, 90% of the sandwiches were stable on the first scan; about half of them could withstand repeated scans. The rectification ratios (RR) ranged between 3 and 12 at 0.7 V. Pushing the bias range to ± 1.0 V, the RR increased to between 50 and 200, but the sandwiches lasted for only a few scans. These results were in good agreement with the results observed in Au|LB $[\text{Fe}^{\text{III}}(\text{L}^6)\text{Cl}]$ Au assemblies previously discussed, considering that the work function of the GaIn electrode is about 4.3 eV,¹³⁵ while the work function of the Au electrode is 5.1 eV. Also similar to the previous study, rectification is ascribed to the population of the $^{\text{H}}\text{Fe}^{\text{III}}$ doubly degenerate $d_{xz}^1 + d_{yz}^1$ SOMO and followed by rapid electron transfer to the Au electrode. This collaboration with the Metzger group enabled an independent monitoring of rectification, and recently we teamed up to study the current rectification behavior of the new $^{\text{H}}\text{Fe}^{\text{III}}$ surfactant¹³⁴ $[\text{Fe}^{\text{III}}(\text{L}^8)(\text{OMe})_2]$, Figure 8g, based on an asymmetric $[\text{N}_3\text{O}]$ ligand containing a pyridine and a phenolate tethered by the usual phenylenediamine bridge. We hypothesized that the incorporation of electron deficient pyridine groups to the ligand framework, even if in six-coordinate environments, would lower the SOMO energy levels and enable directional electron transfer. A preliminary measurement on Au|LB $[\text{Fe}^{\text{III}}(\text{L}^8)(\text{OMe})_2]$ Au performed in our lab led to inconclusive results and we opted to use an EGaIn/Ga₂O₃|LB $[\text{Fe}^{\text{III}}(\text{L}^8)(\text{OMe})_2]$ Au assembly. This approach allowed us to compare the results with the recently studied $[\text{Fe}^{\text{III}}(\text{L}^6)\text{Cl}]$ on the same platform. This asymmetric, six-coordinate metallosurfactant behaves as a rectifier with a maximum RR of 300 between +1 and -1 V, in good agreement with the previously studied metallosurfactants $[\text{Fe}^{\text{III}}(\text{L}^6)\text{Cl}]$ and even $[\text{Fe}^{\text{III}}\text{L}^5]$ on gold.

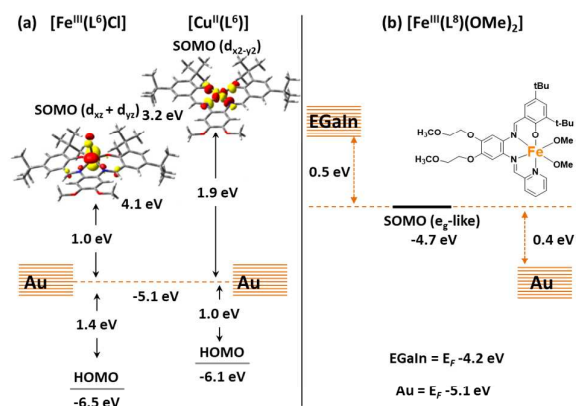


Figure 12. Fermi/SOMO/HOMO arguments for (a) $[\text{Fe}^{\text{III}}(\text{L}^6)\text{Cl}]$ $[\text{Cu}^{\text{II}}(\text{L}^6)]$ in Au|LB|Au and (b) $[\text{Fe}^{\text{III}}(\text{L}^8)(\text{OMe})_2]$ in EGaIn|Lb|Au assemblies.

These results allow for some mechanistic inferences; knowing that E_F energies for EGaIn and Au electrodes reach respectively -4.2 and -5.1 eV below vacuum, we have converted redox potentials measured via cyclic voltammetry to comparable solid-state potentials and obtained a value of -4.7 eV for the SOMO. Considering the pseudo-octahedral geometry of the molecule, this MO is likely found among t_{2g} -like orbitals. Hence, the EGaIn E_F lie *ca.* 0.5 eV above the Fe-based SOMO, whereas the Au E_F lie *ca.* 0.4 V below and electron transfer is certain to occur when an appropriate bias is applied, as summarized in **Figure 12b**. An alternative mechanism may involve electrons from the EGaIn electrode populating higher energy e_g -like SOMOs and forming an excited (Fe^{II})* state in the process. This excited electron can then be transferred to the Au electrode either directly or via d-d decay that lowers the energy of the resulting doubly occupied MO prior to transfer. The ligand-based HOMO lies at *ca.* 1.3 eV below Au. This last study is relevant because it points out to the possibility that orbital distortion alone, as provided by dissimilar donors in a pseudo-octahedral environment may be able to provide enough distortion that enables current rectification at a molecular level.

Several rectifying metallocenes show current alterations upon repeating scans, associated with an increased symmetry in the I/V behavior that eventually culminates in a near-sigmoidal response similar to those described in **Figures 2a** and **11b**. This behavior is tentatively attributed to molecular reorientation in presence of high electric fields.¹³⁶ Reorientation is intended to minimizing the dipole moment in order to decrease the energy of a stable monolayer, and has been observed in organic rectifiers.⁵³

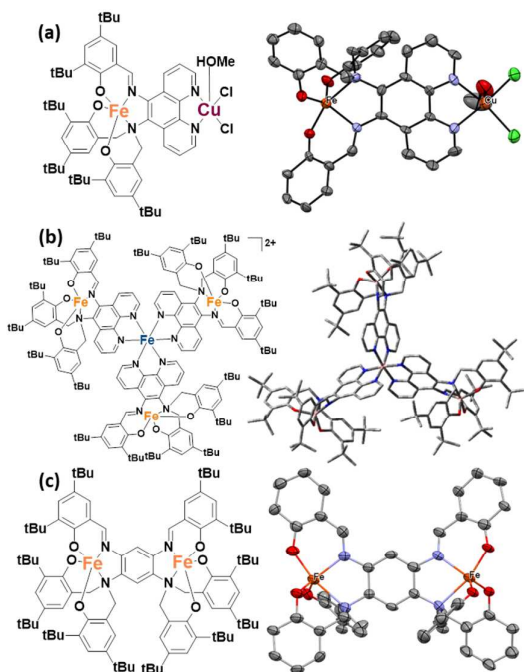


Figure 13. Multimetallic systems for current rectification (a) $[Fe^{III}L^9Cu^I Cl_2 MeOH]$ with X-ray structure, (b) discoid $[(Fe^{III}L^9)_3 Fe^{II}]$ hydrophobe with MM-UFF model, (c) $[Fe^{III}_2(L^{10})]$ hydrophobe with X-ray structure. The *t*-butyl groups are omitted for clarity.

To the best of our knowledge, no *in situ* spectro-electrochemical studies were previously known on the orientation changes of metallocenes deposited as LB film on gold electrode surfaces and upon electrochemical reduction. In collaboration with the Brand group¹³⁷ we have recently analyzed such changes in molecular orientation in a single monolayer of the metallocene $[Fe^{III}L^5]$ by means of IRRAS. As previously detailed, asymmetric rectification involves the lowest lying SOMO, respectively the e'' or e' sets containing $3d_{xz}$ and $3d_{yz}$ in trigonal bipyramidal or square pyramidal symmetry, which receives one electron from the first Au electrode, which is rapidly transferred onto the second Au electrode. The electron transfer associated with Fe^{II} formation triggers large reorientation of the adsorbed metallocene molecules in LB films. This reorientation leads to film desorption at potentials lower than -0.75 V and was originally considered to be the reason for gradual loss of activity. While this issue may indeed have some long-term consequences, the desorbed film is immediately resorbed to the Au surface when direction of the potential scan is reversed. An observed change in orientation of some ligand donors in the vicinity of the metal center was considered more concerning, and implied that the reduction of the $^{55}Fe^{III}$ center in $[Fe^{III}L^5]$ leads to the cleavage of one of the three Fe-O_{phenolate} bonds. This cleavage may be reversible, but will lead to increasing irreversibility. This cleavage also affects the orientation of the hydrophilic alkoxy chains. These sub-molecular changes dependent strongly on the applied potentials and the design of future rectifiers will need to take into account either the limiting potential range in which rectification is attained, or ligand design modifications to prevent donor dissociation.

One possible consequence of electron transport through the SOMOs invoked in the above-described asymmetric mechanisms of rectification observed in five-coordinate $^{55}Fe^{III}$ surfactants, is that the incoming electron originated at the Au electrode will likely be spin polarized. While this possibility seems worth of further evaluation, it may also explain the modest rectification ratios (*RR*) observed for these systems. Aiming to address this issue, we are considering multimetallic species in which the presence of more than one $^{55}Fe^{III}$ center may "amplify" the number of electrons being transferred by molecule. We are building on ligand designs that involve the replacement of the phenylenediamine moiety by a coordinating phenanthroline diamine equivalent. This design maintains a five-coordinate Fe^{III} ion in the usual $[N_2O_3]$ pocket and allows for expansion of the nuclearity through the phenanthroline; a heterometallic, spin-diverse $[Fe^{III}L^9Cu^I Cl_2 MeOH]$ complex¹³⁸ (**Figure 13a**) has been isolated in 2007 as proof-of-concept for selective redox response, and a modular approach was used in 2010 to attain redox-active tetrametallic $[(Fe^{III}L^9)_3 Fe^{II}]$ hydrophobes¹³⁹ of discoid topology (**Figure 13b**). A different strategy involves the use of a new bimetallic hydrophobe $[Fe^{III}_2(L^{10})]$ with an $[N_4O_6]$ bicompartamental topology (**Figure 13c**) capable of accommodating two five-coordinate Fe^{III} ions bridged at a distance of *ca.* 8 Å.¹⁴⁰ This species forms a well-defined PL film at the air-water interface, with collapse pressure of 32 mN/m and leads to Au|LB $[Fe^{III}_2(L^{10})]$ |Au assemblies with *RR* values between 3 and 16. However, an

approximate calculated average area that considers the sectional area of an idealized cylindrical molecule seems slightly larger than the experimentally observed value. This model suggests lack of uniformity, where only certain molecules contact the electrodes directly and preclude assessment of enhancement in rectification behavior. Ligand changes will be necessary in order to improve the amphiphilic character of these hydrophobes, thus enabling better packing.

Conclusions and outlook

We have discussed the initial successes and shortcomings of using LB monolayers of surfactants containing five-coordinate $^{55}\text{Fe}^{\text{III}}$ ions for unidirectional current rectification. Future research will expand on these concepts to probe metal ions such as $^{55}\text{3d}^5\text{Mn}^{\text{II}}$, whose similar electronic distribution in trigonal bipyramidal and square pyramidal fields should mimic closely that of $^{55}\text{Fe}^{\text{III}}$, and evaluate the role of ligand field asymmetry in pseudo-octahedral environments. The use of early transition metals such as $3d^0\text{Sc}^{\text{III}}$, $3d^1\text{Ti}^{\text{III}}$ and $(\text{V}^{\text{IV}}=\text{O})^{2+}$, and $3d^3\text{Cr}^{\text{III}}$ in pseudo-octahedral geometries will further the understanding of electron transfer to, and transport through, singly populated t_{2g} SOMOs. *In-situ* studies on the redox activity of several of these rectifiers will shed further light on how to accomplish more robust systems. Similarly, the ligands intended for polymetallic rectification will require improvements in the amphiphilicity. Even considering such constraints, the iron-based systems discussed here serve as extraordinary tools to enable a fundamental understanding of electron transport mechanisms in 3d metal-based rectifiers.

Conflicts of interest

No conflicts to declare.

Acknowledgements

Over the last 16 years several talented individuals contributed to the development of these ideas: Rajendra Shakya (Ph.D. '07), Jeffery Driscoll (Ph.D. '08), Sarmad Hindo (Ph.D. '09), Rama Shanmugam (Ph.D. '11), Frank Lesh (Ph.D. '12), and Dakshika Wanniarachchi (Ph.D. '14) studied the chemistry of metallosurfactants. Camille Imbert (M.Sc. '05), Mauricio Lanznaster (Ph.D. '04), Marco Allard (Ph.D. '10), Lanka Wickramasinghe (Ph.D. '14), and Sunalee Gonawala (Ph.D. '16) studied all aspects of rectification based on five-coordinate iron surfactants. Isuri Weeraratne ('15), Samudra Amunugama ('16), and Abigail Cousino ('17), continue the discoveries in this fascinating area. Several collaborators have volunteered their knowledge to complement the multidisciplinary nature of this research, among them Sandro da Rocha, Paul Keyes, and Alex Benderskii (initial surfactant studies), Berny Schlegel and Shivnath Mazumder (DFT calculations), Bruce McGarvey (EPR spectroscopy), Mary Jane Heeg (X-ray crystallography), Zhixian Zhou (initial *I/V* curves), Guagzhao Mao and Isabella Brand (surface studies), and Robert Metzger (EGain

rectification studies). The Nano@Wayne initiative (Fund-11E420), and the Donors of the ACS-Petroleum Research Fund (Grant 42575-G3) provided early financial support to this enterprise, which continued through the generous funding of the National Science Foundation through grants NSF-CHE-0718470, NSF-CHE-1012413, and NSF-CHE-1500201.



Claudio Verani got his M.Sc. (1997, honors) with Ademir Neves at the Universidade Federal de Santa Catarina in Brazil. His PhD came under the mentorship of Phalguni Chaudhuri and Karl Wiegardt and at the Max-Planck Institute for Bioinorganic Chemistry and Ruhr Universität-Bochum in Germany, where he developed experimental models to understand magnetic coupling in heteronuclear species. He moved to the US in 2000 for postdoctoral work with Kenneth Karlin at the Johns Hopkins University, modelling aspects of dioxygen activation by Cytochrome-c-oxidase. At Wayne State since 2002, he was promoted to associate professor in 2008 and to professor in 2013. He is also serving as associate dean for research at the WSU - College of Liberal Arts and Sciences since 2017. He and his group utilize a multidisciplinary approach to (i) merge coordination chemistry and surface science for molecular electronics, and (ii) develop $3d^0$ catalysts for water splitting. In his personal time, he enjoys the company of wife, daughter, and dog, learns the bass clarinet, and reads about archaeology and history.

References

- (a) H. Choi and C. C. M. Mody *Soc. Stud. Sci.* 2009, **39**, 11-50; (b) S. Fernbach and W. G. Proctor, *J. Appl. Phys.*, 1955, **26**, 170-181; (c) A. von Hippel *Science* 1956, **123**, 315-317.
- R. Feynman, *Caltech Eng. & Sci. Mag.*, 1960, 22-36.
- G.E. Moore, *Electronics*, 1965, **38**, 114-117.
- A. Aviram, *Int. J. Quantum Chem.*, 1992, **42**, 1615-1624.
- R. L. Carroll and C. B. Gorman, *Angew. Chem. Int. Ed.*, 2002, **41**, 4378-4400.
- M. C. Petty, *Molecular Electronics: From Principles to Practice: Wiley Series in Materials for Electronic & Optoelectronic Applications*, 2007.
- K. Szacilowski, *Infochemistry: information processing at the nanoscale*, John Wiley & Sons, 2012.
- (a) C. Joachim and M. A. Ratner, *PNAS*, 2005, **102**, 8801-8808; (b) C. Joachim, J. Gimzewski and Aviram, *Nature*, 2000, **408**, 541.
- R. A. Wassel and C. B. Gorman, *Angew. Chem. Int. Ed.*, 2004, **43**, 5120-5123.
- R. M. Metzger, *Chem. Rev.* 2015, **115**, 5056-5115.
- J. Y. Son and H. Song, *Curr. Appl Phys.*, 2013, **13**, 1157-1171.
- P. J. Low, *Dalton Trans.*, 2005, 2821-2824.
- S. J. Higgins and R. J. Nichols, *Polyhedron*, 2018, **140**, 25-34.
- W. J. Pietro, *Adv Mater.*, 1994, **6**, 239-242.
- S. Roth, S. Blumentritt, M. Burghard, C. Fischer, G. Philipp and C. Müller-Schwanneke, *Synth. Met.*, 1997, **86**, 2415-2418.
- G. J. Ashwell, B. Urasinska and W. D. Tyrrell, *Phys. Chem. Chem. Phys.*, 2006, **8**, 3314-3319.
- M.-H. Yoon, A. Facchetti and T. J. Marks, *PNAS*, 2005, **102**, 4678-4682.
- K. Padmaja, W. J. Youngblood, L. Wei, D. F. Bocian and J. S. Lindsey, *Inor. Chem.*, 2006, **45**, 5479-5492.

19. D. Holten, D. F. Bocian and J. S. Lindsey, *Acc. Chem. Res.*, 2002, **35**, 57-69.
20. J. Park, A. N. Pasupathy, J. I. Goldsmith, C. Chang, Y. Yaish, J. R. Petta, M. Rinkoski, J. P. Sethna, H. D. Abruña and P. L. McEuen, *Nature*, 2002, **417**, 722.
21. K. Seo, A. V. Konchenko, J. Lee, G. S. Bang and H. Lee, *J. Am. Chem. Soc.*, 2008, **130**, 2553-2559.
22. J. Lee, H. Chang, S. Kim, G. S. Bang and H. Lee, *Angew. Chem. Int. Ed.*, 2009, **48**, 8501-8504.
23. R. A. Wassel, R. R. Fuierer, N. Kim and C. B. Gorman, *Nano Lett.*, 2003, **3**, 1617-1620.
24. R. A. Wassel, G. M. Credo, R. R. Fuierer, D. L. Feldheim and C. B. Gorman, *J. Am. Chem. Soc.*, 2004, **126**, 295-300.
25. R. Mas-Ballesté, J. Gómez-Herrero and F. Zamora, *Chem. Soc. Rev.*, 2010, **39**, 4220-4233.
26. K. Pilarczyk, B. Daly, A. Podborska, P. Kwolek, V. A. Silversson, A. P. de Silva and K. Szaciłowski, *Coord. Chem. Rev.*, 2016, **325**, 135-160.
27. Z. Yi, S. Trellenkamp, A. Offenhäusser and D. Mayer, *Chem. Commun.*, 2010, **46**, 8014-8016.
28. S. Chappell, C. Brooke, R. J. Nichols, L. J. K. Cook, M. Halcrow, J. Ulstrup and S. J. Higgins, *Faraday Discuss.*, 2016, **193**, 113-131.
29. L. Luo, L. Balhorn, B. Vlaisavljevich, D. Ma, L. Gagliardi and C. D. Frisbie, *J. Phys. Chem. C*, 2014, **118**, 26485-26497.
30. S. Rigaut, *Dalton Trans.*, 2013, **42**, 15859-15863.
31. G. De Ruiter and M. E. Van Der Boom, *J. Mater. Chem.*, 2011, **21**, 17575-17581.
32. C. Toher, D. Nozaki, G. Cuniberti and R. M. Metzger, *Nanoscale*, 2013, **5**, 6975-6984.
33. M. Warzecha, M. Oszejca, K. Pilarczyk and K. Szaciłowski, *Chem. Commun.*, 2015, **51**, 3559-3561.
34. J. S. Lindsey and D. F. Bocian, *Acc. Chem. Res.*, 2011, **44**, 638-650.
35. T. Nagashima, H. Ozawa, T. Suzuki, T. Nakabayashi, K. Kanaizuka and M. A. Haga, *Chem. Eur. J.*, 2016, **22**, 1658-1667.
36. D. B. Strukov, G. S. Snider, D. R. Stewart and R. S. Williams, *Nature*, 2008, **453**, 80.
37. A. Bandyopadhyay, S. Sahu and M. Higuchi, *J. Am. Chem. Soc.*, 2011, **133**, 1168-1171.
38. N. D. Paul, U. Rana, S. Goswami, T. K. Mondal and S. Goswami, *J. Am. Chem. Soc.*, 2012, **134**, 6520-6523.
39. M. Nishikawa, K. Nomoto, S. Kume and H. Nishihara, *J. Am. Chem. Soc.*, 2012, **134**, 10543-10553.
40. J. Ponce, C. R. Arroyo, S. Tatay, R. Frisenda, P. Gaviña, D. Aravena, E. Ruiz, H. S. Van Der Zant and E. Coronado, *J. Am. Chem. Soc.*, 2014, **136**, 8314-8322.
41. M. F. Oszejca, K. L. McCall, N. Robertson and K. Szaciłowski, *J. Phys. Chem. C*, 2011, **115**, 12187-12195.
42. M. Castellano, R. Ruiz-Garcia, J. Cano, J. Ferrando-Soria, E. Pardo, F. R. Fortea-Pérez, S.-E. Stiriba, W. P. Barros, H. O. Stumpf and L. Cañadillas-Delgado, *Coord. Chem. Rev.*, 2015, **303**, 110-138.
43. R. M. Metzger, *Nanoscale*, 2018, **10**, 10316-10332.
44. M. Ratner and A. Aviram, *Chem. Phys. Lett.*, 1974, **29**, 277-283.
45. The electrode|molecule|electrode junction is also defined as a sandwich. In this work junctions and sandwiches will be referred to as "assemblies".
46. I. Franco, G. C. Solomon, G. C. Schatz and M. A. Ratner, *J. Am. Chem. Soc.*, 2011, **133**, 15714-15720.
47. G. J. Ashwell, B. Urasinska-Wojcik and L. J. Phillips, *Angew. Chem. Int. Ed.*, 2010, **122**, 3586-3590.
48. A. Troisi and M. A. Ratner, *Nano Lett.*, 2004, **4**, 591-595.
49. A. Troisi and M. A. Ratner, *J. Am. Chem. Soc.*, 2002, **124**, 14528-14529.
50. V. Mujica, M. Kemp, A. Roitberg and M. Ratner, *J. Chem. Phys.*, 1996, **104**, 7296-7305.
51. G. J. Ashwell, J. R. Sambles, A. S. Martin, W. G. Parker and M. Szablewski, *J. Chem. Soc. Chem. Commun.*, 1990, DOI: 10.1039/C39900001374, 1374-1376.
52. A. S. Martin, J. R. Sambles and G. J. Ashwell, *Phys. Rev. Lett.*, 1993, **70**, 218-221.
53. R. M. Metzger, B. Chen, U. Höpfner, M. V. Lakshmikantham, D. Vuillaume, T. Kawai, X. Wu, H. Tachibana, T. V. Hughes, H. Sakurai, J. W. Baldwin, C. Hosch, M. P. Cava, L. Brehmer and G. J. Ashwell, *J. Am. Chem. Soc.*, 1997, **119**, 10455-10466.
54. C. Krzeminski, C. Delerue, G. Allan, D. Vuillaume and R. M. Metzger, *Phys. Rev. B*, 2001, **64**, 085405.
55. R. M. Metzger, *Acc. Chem. Res.*, 1999, **32**, 950-957.
56. R. M. Metzger, *Chem. Rev.*, 2003, **103**, 3803-3834.
57. R. M. Metzger, *Chem. Rec.*, 2004, **4**, 291-304.
58. R. M. Metzger, *J. Mater. Chem.*, 2008, **18**, 4364-4396.
59. O. A. Al-Owaedi, D. C. Milan, M.-C. Oerthel, S. Bock, D. S. Yufit, J. A. K. Howard, S. J. Higgins, R. J. Nichols, C. J. Lambert, M. R. Bryce and P. J. Low, *Organometallics*, 2016, **35**, 2944-2954.
60. S. V. Aradhya and L. Venkataraman, *Nat. Nanotech.*, 2013, **8**, 399.
61. R. Davidson, O. A. Al-Owaedi, D. C. Milan, Q. Zeng, J. Tory, F. Hartl, S. J. Higgins, R. J. Nichols, C. J. Lambert and P. J. Low, *Inorg. Chem.*, 2016, **55**, 2691-2700.
62. I. Díez-Pérez, J. Hihath, Y. Lee, L. Yu, L. Adamska, M. A. Kozhushner, I. I. Oleynik and N. Tao, *Nat. Chem.*, 2009, **1**, 635.
63. A. Pablo, A.-O. Pilar, S. J. M., P. J. José, G.-H. Julio and Z. Félix, *Adv. Mater.*, 2018, **30**, 1705645.
64. F. Schwarz, G. Kastlunger, F. Lissel, C. Egler-Lucas, S. N. Semenov, K. Venkatesan, H. Berke, R. Stadler and E. Lörtscher, *Nat. Nanotech.*, 2015, **11**, 170.
65. G. J. Ashwell and A. Mohib, *J. Am. Chem. Soc.*, 2005, **127**, 16238-16244.
66. Y. Liu, Y. Xu, J. Wu and D. Zhu, *Solid State Commun.*, 1995, **95**, 695-699.
67. Y. Liu, Y. Xu and D. Zhu, *Synth. Met.*, 1997, **90**, 143-146.
68. B. Capozzi, J. Xia, O. Adak, E. J. Dell, Z.-F. Liu, J. C. Taylor, J. B. Neaton, L. M. Campos and L. Venkataraman, *Nat. Nanotech.*, 2015, **10**, 522.
69. (a) M. L. Chabinyx, X. Chen, R. E. Holmlin, H. Jacobs, H. Skulason, C. D. Frisbie, V. Mujica, M. A. Ratner, M. A. Rampi and G. M. Whitesides, *J. Am. Chem. Soc.*, 2002, **124**, 11730-11736; (b) V. Mujica, M. A. Ratner and A. Nitzan, *Chem. Phys.*, 2002, **281**, 147-150.
70. (a) P. E. Kornilovitch, A. M. Bratkovsky, and R. Stanley Williams *Physical Review B* 2002, **66**, 165436; (b) C. A. Nijhuis, W. F. Reus, and G. M. Whitesides *J. Am. Chem. Soc.* 2010, **132**, 18386-18401.
71. N. Nerngchamngong, L. Yuan, D.-C. Qi, J. Li, D. Thompson and C. A. Nijhuis, *Nat. Nanotech.*, 2013, **8**, 113.
72. S.-K. Oh, L. A. Baker and R. M. Crooks, *Langmuir*, 2002, **18**, 6981-6987.
73. A. Omar, Á. Marta, A.-K. A. I., Y. Basit and K. Wolfgang, *Adv. Func. Mater.*, 2008, **18**, 3487-3496.
74. G. J. Ashwell, B. J. Robinson, M. A. Amiri, D. Locatelli, S. Quici and D. Roberto, *J. Mater. Chem.*, 2005, **15**, 4203-4205.
75. C. P. Collier, G. Mattersteig, E. W. Wong, Y. Luo, K. Beverly, J. Sampaio, F. M. Raymo, J. F. Stoddart and J. R. Heath, *Science*, 2000, **289**, 1172-1175.

76. A. Jaiswal, D. Rajagopal, M. V. Lakshmikantham, M. P. Cava and R. M. Metzger, *Phys. Chem. Chem. Phys.*, 2007, **9**, 4007-4017.
77. N. Man-Kit and Y. Luping, *Angew. Chem. Int. Ed.*, 2002, **41**, 3598-3601.
78. X. Tao, P. I. R., L. M. V. and M. R. M., *Angew. Chem. Int. Ed.*, 2001, **40**, 1749-1752.
79. Y. Jie-Wen, C. Antoinette, R. T. Y., X. Guo-Lin and R. Tong, *Chem. Eur. J.*, 2007, **13**, 6874-6882.
80. Y. Lee, S. Yuan, A. Sanchez and L. Yu, *Chem. Commun.*, 2008, DOI: 10.1039/B712978E, 247-249.
81. S. Sun, X. Zhuang, L. Wang, B. Zhang, J. Ding, F. Zhang and Y. Chen, *Journal of Materials Chemistry C*, 2017, **5**, 2223-2229.
82. J. Jiang, J. A. Spies, J. R. Swierk, A. J. Matula, K. P. Regan, N. Romano, B. J. Brennan, R. H. Crabtree, V. S. Batista, C. A. Schmuttenmaer and G. W. Brudvig, *J. Phys. Chem. C*, 2018, **122**, 13529-13539.
83. H. Murni, G. Syun, T. Daisuke and O. Takuji, *Chem. Eur. J.*, 2014, **20**, 7655-7664.
84. R. Liu, S.-H. Ke, W. Yang and H. U. Baranger, *J. Chem. Phys.*, 2006, **124**, 024718.
85. W. J. Shumate, D. L. Mattern, A. Jaiswal, D. A. Dixon, T. R. White, J. Burgess, A. Honciuc and R. M. Metzger, *J. Phys. Chem. B*, 2006, **110**, 11146-11159.
86. E. D. Mentovich, N. Rosenberg-Shraga, I. Kalifa, M. Gozin, V. Mujica, T. Hansen and S. Richter, *J. Phys. Chem. C*, 2013, **117**, 8468-8474.
87. J. Hyunhak, K. Dongku, W. Gunuk, P. Sungjun, L. Hanki, C. Kyungjune, H. Wang-Taek, Y. Myung-Han, J. Y. Hee, S. Hyunwook, X. Dong and L. Takhee, *Adv. Funct. Mater.*, 2014, **24**, 2472-2480.
88. (a) M. A. Sierra, D. Sanchez, A. R. Garrigues, E. del Barco, L. Wang and C. A. Nijhuis, *Nanoscale*, 2018, **10**, 3904-3910; (b) L. Yuan, R. Breuer, L. Jiang, M. Schmittel, and C. A. Nijhuis *Nano Lett.* 2015, **15**, 5506-5512.
89. E. A. Osorio, K. Moth-Poulsen, H. S. J. van der Zant, J. Paaske, P. Hedegård, K. Flensburg, J. Bendix and T. Bjørnholm, *Nano Lett.*, 2010, **10**, 105-110.
90. The addition of the name Pockels to the films commonly known as Langmuir monolayers aims to rectify a historical omission towards the pioneering work of Agnes Pockels (1862–1935) in the understanding of film formation at the air/water surface. See the following references: (a) Rayleigh, *Nature*, 1891, **43**, 437-439, (b) A. Pockels, *Nature*, 1892, **46**, 418-419, (c) A. Pockels, *Nature*, 1893, **48**, 152-154, (d) A. Pockels, *Nature* 1894, **50**, 223-224.
91. Although similar isotherms had been investigated by Agnes Pockels and Lord Rayleigh, the research of Irving Langmuir brought unprecedented attention to the field. See I. Langmuir *J. Am. Chem. Soc.* 1917, **39**, 1848-1906
92. G. Roberts, in *Langmuir-Blodgett Films*, Springer, 1990, pp. 317-411.
93. M. C. Petty, *Langmuir-Blodgett films: an introduction*, Cambridge University Press, 1996.
94. A. Ulman, *An Introduction to Ultrathin Organic Films: From Langmuir-Blodgett to Self-Assembly*, Academic press, 2013.
95. H. E. Ries Jr, *Nature*, 1979, **281**, 287.
96. V. M. Kaganer, H. Möhwald and P. Dutta, *Rev. Mod. Phys.*, 1999, **71**, 779-819.
97. S. Ramos and R. Castillo, *J. Chem. Phys.*, 1999, **110**, 7021-7030.
98. See (a) K. B. Blodgett *J. Am. Chem. Soc.*, 1934, **56**, 495 and (b) K. B. Blodgett *J. Am. Chem. Soc.*, 1935, **57**, 1007-1022
99. M. D. Curtis, J. Cao and J. W. Kampf, *J. Am. Chem. Soc.*, 2004, **126**, 4318-4328.
100. H. D. Jayathilake, J. A. Driscoll, A. N. Bordenyuk, L. Wu, S. R. P. da Rocha, C. N. Verani and A. V. Benderskii, *Langmuir*, 2009, **25**, 6880-6886.
101. H. E. Katz, Z. Bao and S. L. Gilat, *Acc. Chem. Res.*, 2001, **34**, 359-369.
102. H. H. J. Kattner, *External reflection spectroscopy of thin films on dielectric substrates: Handbook of vibrational spectroscopy*, John Wiley & Sons Ltd., Chichester, 2002.
103. C. N. Verani, R. Shanmugam, F. R. Xavier, M. M. Allard and K. K. Kpogo, *Dalton Trans.*, 2013, **42**, 15296-15306.
104. P. Eaton and P. West, *Atomic force microscopy*, Oxford University Press, 2010.
105. E. Meyer, *Prog. Surf. Sci.*, 1992, **41**, 3-49.
106. D. Rugar and P. Hansma, *Phys. Today*, 1990, **43**, 23-30.
107. Y. Wang, X. Du, L. Guo and H. Liu, *J. Chem. Phys.*, 2006, **124**, 134706.
108. C. Imbert, H. P. Hratchian, M. Lanznaster, M. J. Heeg, L. M. Hryhorczuk, B. R. McGarvey, H. B. Schlegel and C. N. Verani, *Inorg. Chem.*, 2005, **44**, 7414-7422.
109. R. Shakya, C. Imbert, H. P. Hratchian, M. Lanznaster, M. J. Heeg, B. R. McGarvey, M. Allard, H. B. Schlegel and C. N. Verani, *Dalton Trans.*, 2006, 2517-2525.
110. F. D. Lesh, S. S. Hindo, M. J. Heeg, M. M. Allard, P. Jain, B. Peng, L. Hryhorczuk and C. N. Verani, *Eur. J. Inorg. Chem.*, 2009, 345-356.
111. N. C. Lim, C. B. Ewart, M. L. Bowen, C. L. Ferreira, C. A. Barta, M. J. Adam and C. Orvig, *Inorg. Chem.*, 2008, **47**, 1337-1345.
112. S. Sarkar, A. Mondal, D. Chopra, J. Ribas and K. K. Rajak, *Eur. J. Inorg. Chem.*, 2006, 3510-3516.
113. R. Shakya, M. M. Allard, M. Johann, M. J. Heeg, E. Rentschler, J. M. Shearer, B. McGarvey and C. N. Verani, *Inorg. Chem.*, 2011, **50**, 8356-8366.
114. R. Shakya, S. S. Hindo, L. Wu, M. M. Allard, M. J. Heeg, H. P. Hratchian, B. R. McGarvey, S. R. P. da Rocha and C. N. Verani, *Inorg. Chem.*, 2007, **46**, 9808-9818.
115. S. S. Hindo, R. Shakya, N. S. Rannulu, M. M. Allard, M. J. Heeg, M. T. Rodgers, S. R. P. da Rocha and C. N. Verani, *Inorg. Chem.*, 2008, **47**, 3119-3127.
116. J. A. Driscoll, M. M. Allard, L. Wu, M. J. Heeg, S. R. da Rocha and C. N. Verani, *Chem. Eur. J.*, 2008, **14**, 9665-9674.
117. C. N. Verani, J. Driscoll, P. H. Keyes and M. J. Heeg, *Inorg. Chem.*, 2014, **53**, 5647-5655.
118. J. A. Driscoll, P. H. Keyes, M. J. Heeg, P. A. Heiney and C. N. Verani, *Inorg. Chem.*, 2008, **47**, 7225-7232.
119. K. E. Goodwill, C. Sabatier and R. C. Stevens, *Biochem.*, 1998, **37**, 13437-13445.
120. M. Lanznaster, H. P. Hratchian, M. J. Heeg, L. M. Hryhorczuk, B. R. McGarvey, H. B. Schlegel and C. N. Verani, *Inorg. Chem.*, 2006, **45**, 955-957.
121. $\tau = (\beta - \alpha)/60$, where β is the largest and α is the second largest angles in the coordination sphere. See: A. Addison, T. Rao and J. Reedijk, *Dalton Trans.*, 1984, **5**, 1349-1356.
122. H. Fujii and Y. Funahashi, *Angew. Chem. Int. Ed.*, 2002, **114**, 3790-3793.
123. M. Lanznaster, A. Neves, A. J. Bortoluzzi, B. Szpoganicz and E. Schwingel, *Inorg. Chem.*, 2002, **41**, 5641-5643.
124. A. Machkour, D. Mandon, M. Lachkar and R. Welter, *Eur. J. Inorg. Chem.*, 2005, 158-161.

125. M. M. Allard, J. A. Sonk, M. J. Heeg, B. R. McGarvey, H. B. Schlegel and C. N. Verani, *Angew. Chem. Int. Ed.*, 2012, **51**, 3178-3182.
126. L. D. Wickramasinghe, M. M. Perera, L. Li, G. Mao, Z. Zhou and C. N. Verani, *Angew. Chem. Int. Ed.*, 2013, **125**, 13588-13592.
127. L. D. Wickramasinghe, S. Mazumder, S. Gonawala, M. M. Perera, H. Baydoun, B. Thapa, L. Li, L. Xie, G. Mao, Z. Zhou, H. B. Schlegel and C. N. Verani, *Angew. Chem. Int. Ed.*, 2014, **53**, 14462-14467.
128. (a) L. Zhang, J. A. Bain, J. G. Zhu, L. Abelmann, T. Onoue, *IEEE Trans. Magn.* 2004, **40**, 2549 – 2551; (b) K. Kitagawa, T. Morita, S. Kimura, *Langmuir* 2005, **21**, 10624 – 10631; (c) K. Seo, A. V. Konchenko, J. Lee, G. S. Bang, H. Lee, *J. Am. Chem. Soc.*, 2008, **130**, 2553 – 2559.
129. J. He, Q. Fu, S. Lindsay, J. W. Cizek and J. M. Tour, *J. Am. Chem. Soc.*, 2006, **128**, 14828-14835.
130. K. Hipps, in *Handbook of applied solid state spectroscopy*, Springer, 2006, pp. 305-350.
131. A. Schmidt, N. Armstrong, C. Goeltner and K. Muellen, *J. Phys. Chem.*, 1994, **98**, 11780-11785.
132. L. Scudiero, D. E. Barlow and K. Hipps, *J. Phys. Chem. B*, 2002, **106**, 996-1003.
133. L. D. Wickramasinghe, S. Mazumder, K. K. Kpogo, R. J. Staples, H. B. Schlegel and C. N. Verani, *Chem. Eur. J.*, 2016, **22**, 10786-10790.
134. M. S. Johnson, C. L. Horton, S. Gonawala, C. N. Verani and R. M. Metzger, *Dalton Trans.*, 2018, **47**, 6344-6350.
135. R. C. Chiechi, E. A. Weiss, M. D. Dickey and G. M. Whitesides, *Angew. Chem. Int. Ed.*, 2008, **47**, 142-144.
136. J. Chen, H. Isshiki, C. Baretzky, T. Balashov and W. Wulfhekel, *ACS nano*, 2018, **12**, 3280-3286.
137. I. Brand, J. Juhaniwicz-Debinska, L. Wickramasinghe and C. N. Verani, *Dalton Trans.*, 2018, DOI: 10.1039/C1038DT00333E.
138. M. Lanznaster, M. J. Heeg, G. T. Yee, B. R. McGarvey and C. N. Verani, *Inorg. Chem.*, 2007, **46**, 72-78.
139. F. D. Lesh, R. Shanmugam, M. M. Allard, M. Lanznaster, M. J. Heeg, M. Rodgers, J. M. Shearer and C. N. Verani, *Inorg. Chem.*, 2010, **49**, 7226-7228.
140. A. D. K. I. Weeraratne, H. Baydoun and C. N. Verani, *Dalton Trans.*, 2018, **Submitted**.

Table of Contents

The state-of-the-art of metallorganic-based molecular rectification is reviewed with an emphasis on asymmetric five-coordinate Fe^{III}-containing surfactants in electrode|LB film|electrode assemblies.

